



Simultaneous Detection of Flare-related Decaying and Decayless Kink Oscillations Using Jerk-aware Motion Magnification

Xiaowei Guo¹, Bo Liang¹, Song Feng[✉], Wei Dai, and Yunfei Yang[✉]

Faculty of Information Engineering and Automation, Kunming University of Science and Technology, Kunming 650500, China; feng.song@kust.edu.cn
Received 2022 July 13; revised 2022 September 17; accepted 2022 September 20; published 2022 October 19

Abstract

Kink oscillations of coronal loops are often influenced by external events and this results in various changes of the oscillations. Studying the changes can provide valuable information for understanding kink oscillations. Our observation focuses on a flare region acquired by the Atmospheric Imaging Assembly on the Solar Dynamics Observatory spacecraft on 2016 March 23. There are a bunch of arched loops and an open loop near the region. However, their oscillations show very low amplitudes. So we used the jerk-aware motion method to magnify the weak oscillations. We found that before the flare onset at 02:59 UT, there were some large loops above the arched loops being raised rapidly. The properties of the weak oscillations show clear changes. On the one hand, the oscillations in the arched loops were decayless initially, but both their amplitude and period increased after 02:30 UT and before the flare onset. Once enhanced, the oscillations decayed with time. On the other hand, the oscillations in the open loop were nearly constant before and after 02:30 UT, but their period increased. This means that the changes in periods and amplitudes of oscillations are likely associated with the loops raised before the flare.

Key words: Sun: corona – Sun: oscillations – Sun: flares – waves

1. Introduction

Kink oscillations of coronal loops, called transverse oscillations, are one of the most controversial dynamic phenomena in the coronal magnetic structure (Verwichte et al. 2004; Su et al. 2012b, 2013; Tian et al. 2012; Nakariakov et al. 2016b, 2021; Yuan & Van Doorsselaere 2016; Li et al. 2022). They were first detected by the high-resolution extreme ultra-violet (EUV) imagers from the Corona Detector in the late 1990s (Aschwanden et al. 1999; Handy et al. 1999; Nakariakov et al. 1999). A large number of kink oscillations were then observed by the Atmospheric Imaging Assembly (AIA) on the Solar Dynamics Observatory (SDO) spacecraft (Lemen et al. 2012), which significantly expand our understanding.

The kink oscillations decay rapidly within several oscillation cycles after onset. The oscillation damping, which is interpreted as a mechanism of resonance absorption (Ruderman & Roberts 2002), shows an exponential profile with an initial amplitude from 1 to 10 Mm (Nechaeva et al. 2019). However, the decayless kink oscillations are also seen in the solar corona (Wang et al. 2012; Anfinogentov et al. 2013). These oscillations are smaller in amplitude (<0.5 Mm) and longer in duration, even up to several hours. The period of both decaying and decayless oscillations is about a few minutes. Moreover, the periods are proportional to the lengths of the coronal loops (Anfinogentov et al. 2015; Goddard et al. 2016;

Nechaeva et al. 2019). Sometimes, the kink oscillations can also be changed from a low-amplitude decaying state to a high-amplitude decayless state (Nisticò et al. 2013; Zhang et al. 2020; Mandal et al. 2021).

The most probable mechanisms of the decaying kink oscillations are eruptions and plasma ejections in the low corona, such as a solar flare eruption (Aschwanden & Schrijver 2011; Su et al. 2012a; Chen et al. 2019), a coronal mass ejection (Chen et al. 2008), and a jet (Sarkar et al. 2016; Dai et al. 2021). But the decayless oscillations are not directly related to coronal eruptions and flares (Anfinogentov et al. 2015). The probable excitation mechanisms for decayless oscillations are a self-oscillatory model (Nakariakov et al. 2016a), a periodic footpoint (Afanasyev et al. 2019), or a constant background flow (Karampelas & Van Doorsselaere 2020). However, their triggering mechanisms have not yet been determined.

In this study, we observed both the decaying and decayless kink oscillations during a flare. This may help us better understand the kink oscillations (Arregui 2015; Van Doorsselaere et al. 2020). However, the amplitudes of oscillations are relatively low. We used the jerk-aware motion magnification method to magnify the oscillations. This paper is as follows. Section 2 describes the observations. The jerk-aware method is described and the kink oscillations of the loops are analyzed in Section 3. Section 4 discusses and summarizes our results.

¹ These authors contributed equally to this work.

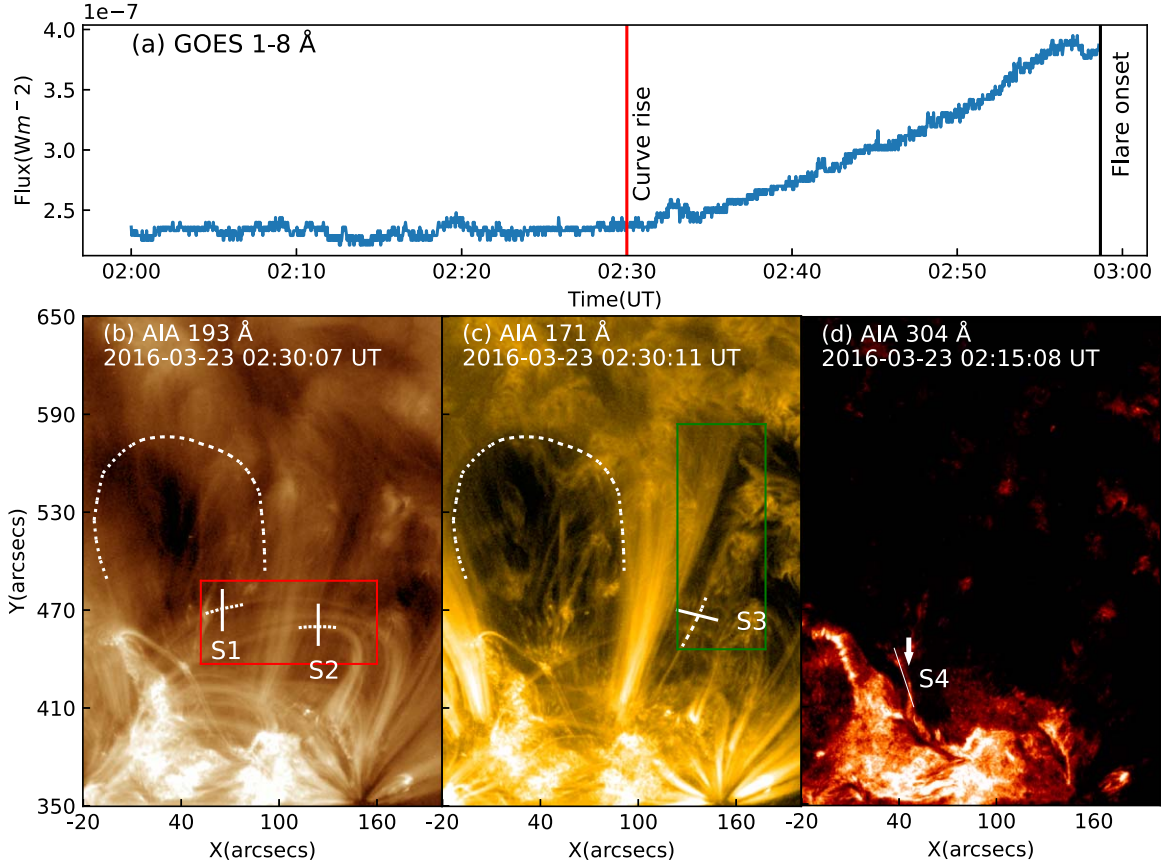


Figure 1. (a) GOES 1–8 Å soft X-ray curve on 2016 March 23. The vertical red and black lines mark the time of the curve rising and the flare onset, respectively. (b)–(d) the 171, 193, and 304 Å images of coronal loops under study. The white lines represent slices S1, S2, S3, and S4, respectively. The white dashed arcs mark the large loops with a bubble-like profile. The red (panel (b)) and green (panel (c)) boxes mark the FOVs of the arched loops and the open loop to be studied in Figures 2 and 3, respectively. The white arrow in panel (d) marks a faint flare ribbon.

2. Observations

In our work, we analyzed the coronal loops of active region (AR) NOAA 12 524 (N20W04) during the solar center on 2016 March 23. The GOES 1–8 Å soft X-ray data is downloaded from 02:00 to 03:00 UT, and meanwhile, the level_1 data were also downloaded between 02:20 and 02:50 UT in the Joint Science Operation Center with 12 s time cadence and $0''.6$ pixel size. Figure 1(a) shows the GOES data (blue line). The curve begins to ascend at 02:30 UT (vertical red line) and a C1.1 flare erupts at 02:59 UT (vertical black line). The time from 02:30 to 02:59 UT is regarded as a preflare phase.

A bundle of the arched loops in 193 Å channel (Figure 1(b)) and an open loop in 171 Å channel (Figure 1(c)) are marked with the white dashed lines, respectively. The open loop presents a visible length with ~ 130 Mm. However, the arched loops are almost invisible in the 171 Å and the open loop is invisible in 193 Å channels. Moreover, the white dashed arcs in Figures 1(b) and (c) mark the large uplifting loops. Meanwhile, Figure 1(d) show a flare ribbon. The animation shows the flare

ribbon gradually forming from 2:20 UT and the large loops with a bubble-like profile start to rise rapidly. They are associated with the flare eruption (Li et al. 2017). Figure 2 shows the evolution of the arched loops located at below the rising loops. After a few minutes, the arched loops also start to uplift slowly and are stretched weakly toward the direction of the top rapid uplift loops. Finally, they gradually disappear from 02:45 UT. Figure 3 shows the time–distance map of the open loop position that is located to the right side of the rapidly rising loops. It moved slowly to its left side and the profile became clearer and clearer with time. Moreover, the period of the open loop becomes longer than before.

3. Data Reduction and Results

3.1. Motion Magnification Method

We noticed the weak kink oscillations in the arched and open loops. However, the displacements of the oscillations are close to the pixel size. So we used the jerk-aware motion magnification method to accentuate the oscillations in the

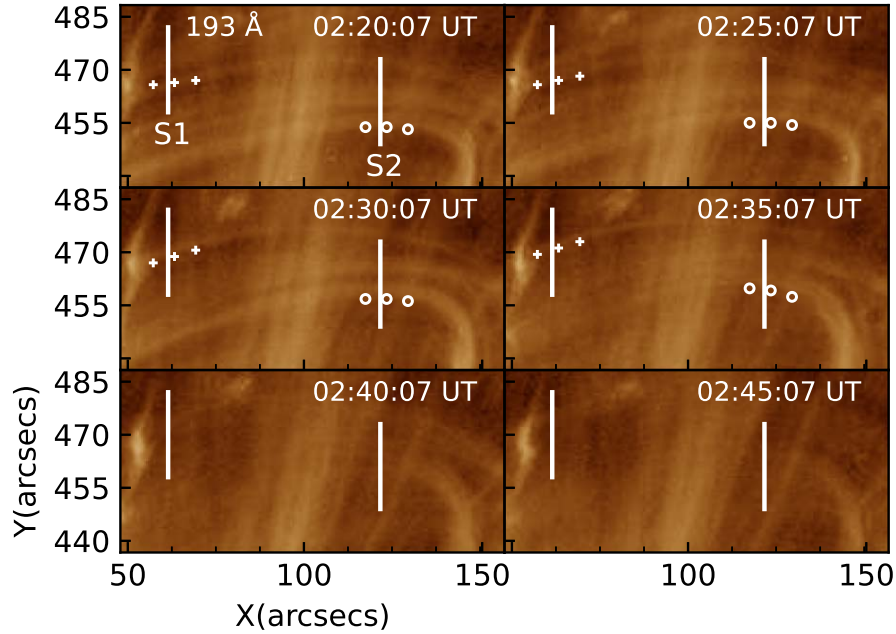


Figure 2. Time evolution of the arched loops, which are shown in Figure 1(b) with a red box. Its FOV is $51'' \times 108''$.

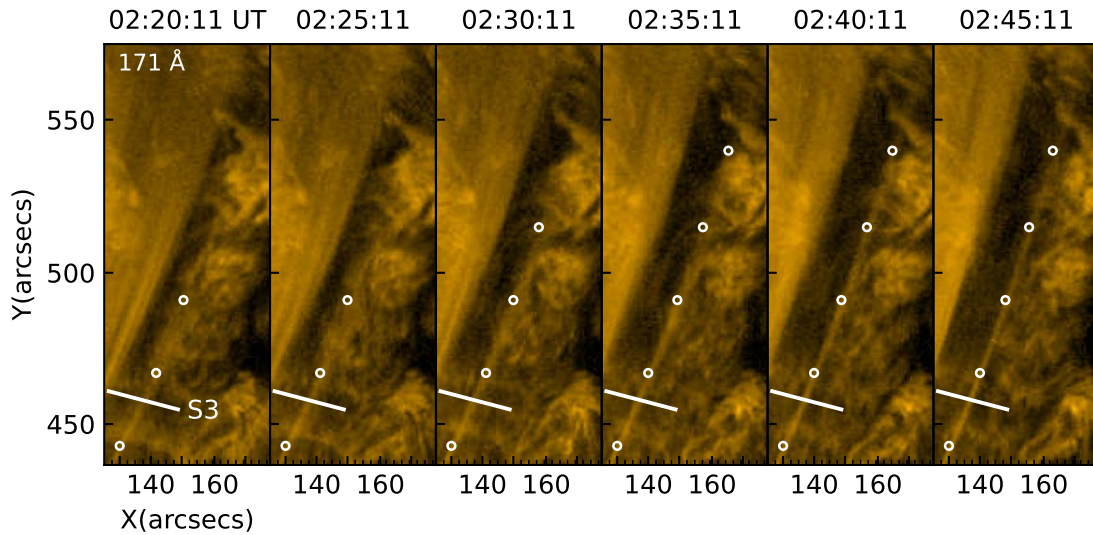


Figure 3. Time evolution of the open loop, which is shown in Figure 1(c) with a green box. Its FOV is $138'' \times 54''$.

image sequence. The jerk-aware method decomposes each image into the complex local wavelet components. Phase information is very sensitive to transverse displacements of different structures in an image, and so, the displacement can be manipulated by the phase information. Therefore, the method extracts the local phase and magnifies them. In that case, we get a motion-magnified image sequence after performing the magnification and reconstructing each image.

For a detailed description of the jerk-aware method, see the literature described by Takeda et al. (2018).

We used simulated oscillation data to validate the effectiveness of the method. Figure 4(a) shows an image containing three loops. Loop 1 oscillates in two stages. The first stage is decayless with 0.2 pixel amplitude and 30 frame period. The second stage is decaying with 1 pixel initial amplitude and 50 frame damping times, but the period remains unchanged. Loop

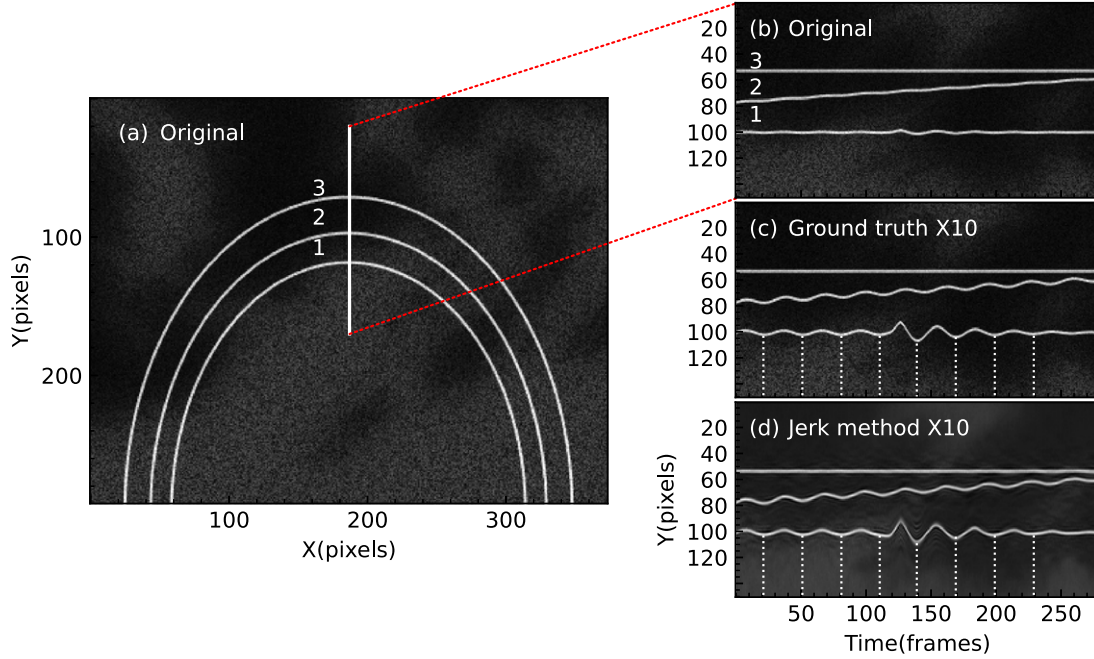


Figure 4. Detection of synthetic oscillations. (a) The simulated loop with three loops. Loop 1 performs successively decayless and decaying oscillations. Loop 2 performs decayless oscillation with the increasing loop major radius. Loop 3 is not oscillating. (b) The original time–distance maps. Similar to (b), panels (c) and (d) are the magnified results of the ground truth and the jerk-aware method, respectively. The white dotted lines mark the position of the oscillations.

2 expands with time, similar to the outline of a semicircle with an increasing radius. At the same time, the loop performs decayless oscillation with 0.2 pixel amplitude, but its oscillation period becomes larger than before. To Loop 3, it has no oscillations.

Figure 4(b) shows the time–distance maps of the three oscillations. Loop 1 performs decayless oscillation before the 100th frame, and then the amplitude is magnified after the 100th frame and disappeared until the 250th frame. Loop 2 presents a decayless loop, but its amplitude is so small that the oscillation cannot be seen. Loop 3 is stable in all the time region. Figure 4(c) presents the map of the magnified oscillations with 10 times the actual amplitude. Figure 4(d) shows the results magnified by the jerk-aware motion magnification method with 10 times the actual amplitude. The white dotted lines in Figures 4(c) and (d) mark the same position. We see that the two maps are the same. After the 100th frame the amplitude gets to increase sharply, and then decays. However, the oscillation disappears after the 250th frame. This prove that the jerk-aware method does not change the period and the phase of the oscillation.

3.2. Oscillation Extraction and Analysis

To highlight the oscillations in the EUV loops, we magnify the oscillations 10 times the actual amplitude. Figures 5(a)–(f) show the maps of Slices S1–S3. The decaying and decayless

oscillations are marked with the purple and cyan signs, respectively. Figures 5(a), (c), and (e) are the original maps and Figures 5(b), (d), and (f) are the magnified maps. Figure 5(g) shows that a flare ribbon begins to brighten from 02:20 UT. The oscillations of slices S1 and S2 are weak and constant initially. However, significantly higher amplitudes and larger periods are observed after 02:30 UT than before. Subsequently, the enhanced oscillations decay with time. Meanwhile, the oscillations in Slice S3 show the period increasing obviously and the amplitude keeping nearly unchanged.

To understand the properties of the kink oscillations in the EUV coronal loops, we obtained the oscillation positions and removed the linear trends. A sine function fitting the decayless oscillations is defined as follows:

$$F(t) = A_1 \sin\left(\frac{2\pi}{P_1}t + \theta_1\right), \quad (1)$$

where A_1 denotes the amplitude, P_1 the period of the oscillations. The decaying sine function is defined as:

$$F(t) = A_2 e^{-\frac{t}{\tau}} \sin\left(\frac{2\pi}{P_2}t + \theta_2\right), \quad (2)$$

where A_2 , P_2 , and τ represent the initial amplitude, period, and damping time, respectively. Table 1 lists the detailed parameters of the sine functions. It notes that the magnified amplitudes have been scaled down to the corresponding original data.

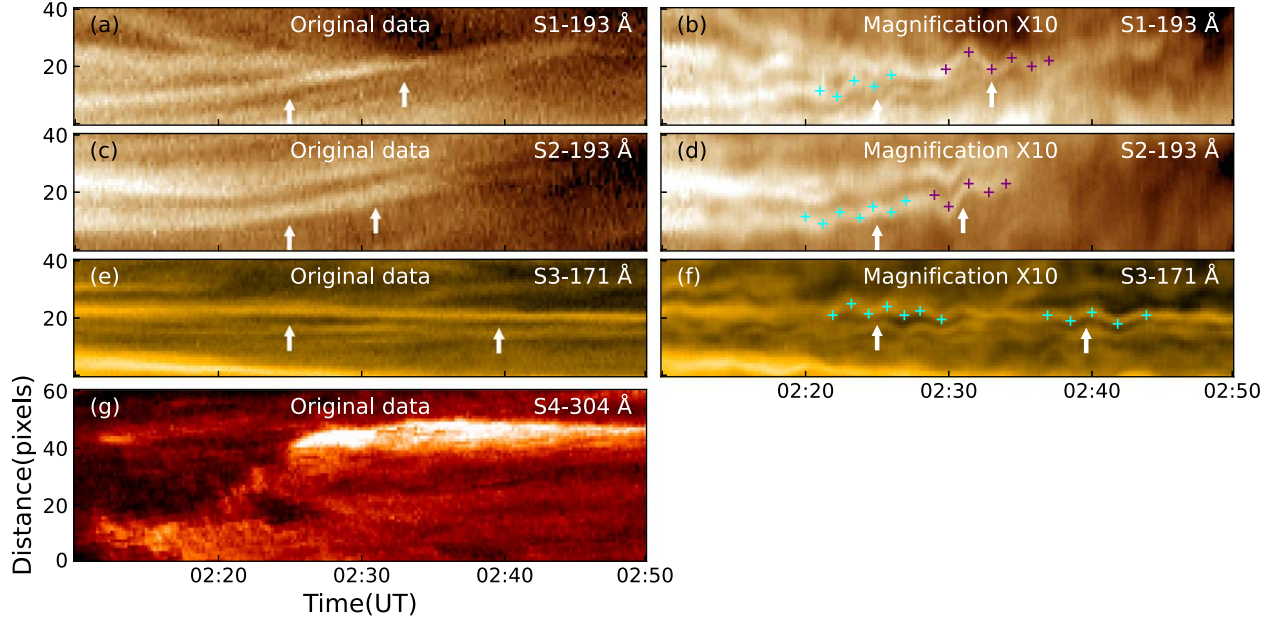


Figure 5. The oscillations maps (a)–(f) and the time evolution map of the flare ribbon (g). (a)–(f) The time–distance and magnified maps magnified by the jerk-aware method, respectively. The white arrows show the positions of the loops. The cyan pluses mark the decayless oscillations and the purple pluses mark the decaying oscillations in (a)–(d). The cyan pluses mark the oscillations in (e) and (f) that are decayless.

Table 1
Parameters of the Sine Fit

Name	A_1 (Mm)	P_1 (s)	A_2 (Mm)	P_2 (s)	τ (s)	τ/P_2
S1	0.065 ± 0.011	158.3 ± 9	0.167 ± 0.03	188.3 ± 7	287.8 ± 58	1.5
S2	0.057 ± 0.006	143.6 ± 7	0.177 ± 0.04	173.3 ± 7	238.3 ± 65	1.4
S3-X1	0.054 ± 0.011	147.0 ± 5
S3-X2	0.057 ± 0.006	228.3 ± 6

Figures 6(a) and (b) show the detrended fitting curves of the oscillations with about 0.065 ± 0.011 and 0.057 ± 0.006 Mm amplitudes and 158.3 ± 9 and 143.6 ± 7 s periods before 02:30 UT. The flare then increases the oscillation amplitude and period of the arched loops. Their periods are 188.3 ± 7 and 173.3 ± 7 s and their amplitudes are 0.167 ± 0.03 and 0.177 ± 0.04 Mm, respectively. The values τ are 287.8 ± 58 and 238.3 ± 65 s in Slices S1 and S2, respectively. Moreover, the damping τ/p_2 in Figure 6(a) is similar to that in Figure 6(b).

Figure 6(c) shows the fitting curves of Slice S3. The fits are about 02:22–02:30 UT and 02:37–02:44 UT and show complete decayless oscillations. Figure 6(c) shows the red curves with about 0.054 ± 0.011 and 0.057 ± 0.006 Mm amplitudes and 147.0 ± 5 and 228.3 ± 6 s periods. The periods increase from about 147 s to about 228 s during two time intervals, but the amplitudes do not change. These results demonstrate the flare causes different effects on coronal loop oscillations.

4. Discussions and Conclusions

We observed a flare and the kink oscillations using the GOES and SDO/AIA data in the AR NOAA 12 524 on 2016 March 23. There are a bunch of arched loops and an open loop near the flare region. The oscillation amplitudes of the loops are too low to be identified. Thus, we used the jerk-aware motion magnification method to identify the weak oscillations. We found that the larger loops uplifting rapidly above the arched loops between 02:30 and 02:59 UT. The time is the preflare phase. The properties of the weak oscillations show clear changes. The arched loops oscillate in decayless and decaying regimes in successive time intervals, while the oscillation of the open loop is decayless. During this process, the periods and amplitudes of the oscillations in arched loops become larger, but the open loop oscillation only increases the period and its amplitude remains unchanged.

The changes in period and amplitude of oscillations are likely associated with the large loops raised before the flare.

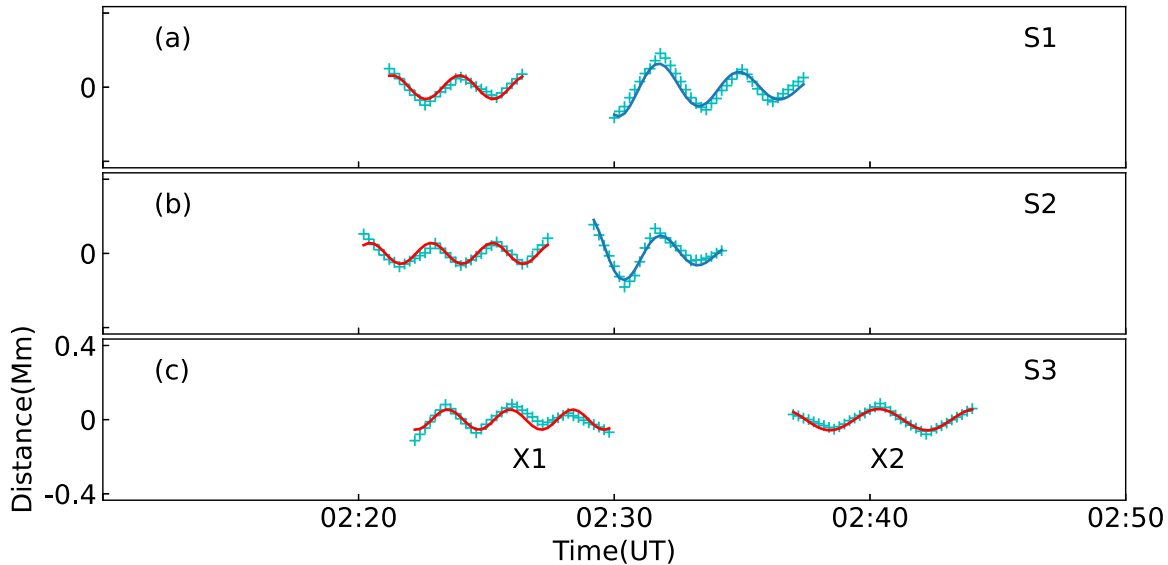


Figure 6. The detrended fitting curves of Slices S1, S2, and S3. The cyan pluses represent the position information of the coronal loops. The red curves represent the results of sine fitting of the decayless oscillations. The blue curves represent the results of sine fitting of the decaying oscillations.

The period of kink oscillations is proportional to the loop length (Anfinogentov et al. 2015; Nechaeva et al. 2019). In our case, the large loops uplifted first. Then the lower arched loops also begin to raise and stretch slightly toward the larger loops. This phenomenon implies that the larger loops above confine the uplift of the lower arched loops. As the larger loops are raised, this limitation disappears and the arched loops are also raised. Meanwhile, the open loop is the lower right side part of the raised loops. These loops are longer than before after being raised and cause the oscillation periods to increase. Moreover, the observed decaying oscillations in the arched loops are likely associated with the resonance of the oscillations. On the one hand, the length of the arched ring is relatively short. This leads to the possibility that energy propagation in the arched loops may trigger resonance. The resonance leads to an increase in the amplitude of the oscillations. On the other hand, the length of the open loop is extremely long. The resonance in the open loop may not be as clear as that in the arched loops. The results imply the large raised loops imposed a larger influence on the arched loops than on the open loop.

Finally, we particularly point out that our finding benefits from the excellent performance of the jerk-aware acceleration magnification method. The jerk-aware method is able to accurately extract the feature changes of small motions, such as the low-amplitude kink oscillations in the solar atmosphere.

Acknowledgments

We thank the reviewer for constructive comments. We thank the GOES and SDO/AIA science teams. S. Feng is supported by the Joint Funds of the National Natural Science Foundation

of China (NSFC, U1931107). W. Dai thanks the NSFC (12063003).

ORCID iDs

Song Feng  <https://orcid.org/0000-0003-4709-7818>

Yunfei Yang  <https://orcid.org/0000-0001-9927-7541>

References

- Afanasyev, A., Karamelas, K., & Van Doorselaere, T. 2019, *ApJ*, **876**, 100
- Anfinogentov, S., Nisticò, G., & Nakariakov, V. M. 2013, *A&A*, **560**, A107
- Anfinogentov, S. A., Nakariakov, V. M., & Nisticò, G. 2015, *A&A*, **583**, A136
- Arregui, I. 2015, *RSPTA*, **373**, 20140261
- Aschwanden, M. J., Fletcher, L., Schrijver, C. J., & Alexander, D. 1999, *ApJ*, **520**, 880
- Aschwanden, M. J., & Schrijver, C. J. 2011, *ApJ*, **736**, 102
- Chen, P. F., Innes, D. E., & Solanki, S. K. 2008, *A&A*, **484**, 487
- Chen, X., Yan, Y., Tan, B., et al. 2019, *ApJ*, **878**, 78
- Dai, J., Zhang, Q. M., Su, Y. N., & Ji, H. S. 2021, *A&A*, **646**, A12
- Goddard, C. R., Nisticò, G., Nakariakov, V. M., & Zimovets, I. V. 2016, *A&A*, **585**, A137
- Handy, B. N., Acton, L. W., Kankelborg, C. C., et al. 1999, *SoPh*, **187**, 229
- Karamelas, K., & Van Doorselaere, T. 2020, *ApJL*, **897**, L35
- Lemen, J. R., Title, A. M., Akin, D. J., et al. 2012, *SoPh*, **275**, 17
- Li, D., Xue, J., Yuan, D., & Ning, Z. 2022, *SCPMA*, **65**, 239611
- Li, Y., Sun, X., Ding, M. D., Qiu, J., & Priest, E. R. 2017, *ApJ*, **835**, 190
- Mandal, S., Tian, H., & Peter, H. 2021, *A&A*, **652**, L3
- Nakariakov, V. M., Anfinogentov, S. A., Antolin, P., et al. 2021, *SSRv*, **217**, 73
- Nakariakov, V. M., Anfinogentov, S. A., Nisticò, G., & Lee, D. H. 2016a, *A&A*, **591**, L5
- Nakariakov, V. M., Ofman, L., Deluca, E. E., Roberts, B., & Davila, J. M. 1999, *Sci*, **285**, 862
- Nakariakov, V. M., Pilipenko, V., Heilig, B., et al. 2016b, *SSRv*, **200**, 75
- Nechaeva, A., Zimovets, I. V., Nakariakov, V. M., & Goddard, C. R. 2019, *ApJS*, **241**, 31
- Nisticò, G., Nakariakov, V. M., & Verwichte, E. 2013, *A&A*, **552**, A57
- Ruderman, M. S., & Roberts, B. 2002, *ApJ*, **577**, 475

- Sarkar, S., Pant, V., Srivastava, A. K., & Banerjee, D. 2016, *SoPh*, **291**, 3269
- Su, J. T., Liu, Y., Liu, S., et al. 2013, *ApJ*, **762**, 42
- Su, J. T., Shen, Y. D., & Liu, Y. 2012a, *ApJ*, **754**, 43
- Su, J. T., Shen, Y. D., Liu, Y., Liu, Y., & Mao, X. J. 2012b, *ApJ*, **755**, 113
- Takeda, S., Okami, K., Mikami, D., Isogai, M., & Kimata, H. 2018, in Proc. IEEE Conf. on Computer Vision and Pattern Recognition, 1769
- Tian, H., McIntosh, S. W., Wang, T., et al. 2012, *ApJ*, **759**, 144
- Van Doorselaere, T., Srivastava, A. K., Antolin, P., et al. 2020, *SSRv*, **216**, 140
- Verwichte, E., Nakariakov, V. M., Ofman, L., & Deluca, E. E. 2004, *SoPh*, **223**, 77
- Wang, T., Ofman, L., Davila, J. M., & Su, Y. 2012, *ApJL*, **751**, L27
- Yuan, D., & Van Doorselaere, T. 2016, *ApJS*, **223**, 24
- Zhang, Q. M., Dai, J., Xu, Z., et al. 2020, *A&A*, **638**, A32